

Article

Photosensitive Spherical Polymer Brushes: Light-Triggered Process of Particle Repulsion

Marek Bekir , Sarah Loebner, Alexej Kopyshv, Nino Lomadze and Svetlana Santer * 

Smart Soft Matter, Institute of Physics and Astronomy, University of Potsdam, 14476 Potsdam, Germany

* Correspondence: santer@uni-potsdam.de

Abstract: We report on a light-triggered process at which repulsive interactions between microparticles with a polyelectrolyte (PE) brush coating can be remotely controlled. The spherical polyelectrolyte brushes are loaded with photosensitive azobenzene containing surfactant which can undergo reversible photo-isomerization from *trans* to *cis* state. The surfactant hydrophilicity is altered by illumination with light of an appropriate wavelength, at which a dynamic exchange of the more surface-active *trans* isomer in comparison to the more water soluble *cis* isomer with the PE brush generates a concentration gradient of the *cis* isomers near a solid surface where the particle is sedimented. In this way, each spherical brush produces its local lateral diffusioosmotic flow pointing outside in a radial direction resulting in mutual long-range repulsive interactions. We demonstrate that a PE layer has a higher tendency to absorb surfactant in comparison to plain silica particles, yielding a larger flow strength. This correlation holds true up to a critical intensity, where the dynamic exchange is adsorption limited with respect to *trans* isomers and especially pronounced for the PE-coated particles.

Keywords: azobenzene containing cationic surfactants; polyelectrolyte brush; spherical brush; colloids; light induced motion of particles; light-driven diffusioosmosis



Citation: Bekir, M.; Loebner, S.; Kopyshv, A.; Lomadze, N.; Santer, S. Photosensitive Spherical Polymer Brushes: Light-Triggered Process of Particle Repulsion. *Processes* **2023**, *11*, 773. <https://doi.org/10.3390/pr11030773>

Academic Editor: Urszula Bazylinska

Received: 23 January 2023

Revised: 24 February 2023

Accepted: 1 March 2023

Published: 6 March 2023



Copyright: © 2023 by the authors. Licensee MDPI, Basel, Switzerland. This article is an open access article distributed under the terms and conditions of the Creative Commons Attribution (CC BY) license (<https://creativecommons.org/licenses/by/4.0/>).

1. Introduction

Spherical polyelectrolyte brushes (SPBs) consist of polyelectrolyte chains covalently grafted to a curved surface of nanoparticles or microparticles [1,2]. One of the ways to synthesize SPBs is the “grafting from” approach, where first, small initiator molecules are attached to a particle surface followed by the growing of polymer chains directly out of the surface [3–11]. When the brush is placed in water most of the counterions are trapped within the shell, building up high osmotic pressure (osmotic limit) and thus resulting in a swelling of the brush [12–14]. In addition, the ionizable groups on a polymer offer a possibility to modify SPBs a posteriori by electrostatic coupling with surfactants, proteins, or nanoparticles or by using them as nanoreactors for the generation of metallic and oxidic nanoparticles [15–24]. During the uptake of, for instance, surfactants, the native counterions of the brush are released owing to an overall gain in entropy [25–30]. This may result in shrinkage of the brush due to the drop in the osmotic pressure or even the overcharging of the polymer shell [31–33]. In this way, SPBs can be considered to be a smart/responsive material, since they can drastically react to variations in environmental conditions (the presence of surfactants, proteins, and so on) or even tiny changes in pH or in the ionic strength of the solution [34–39]. However, SPBs can do even more; namely, they can pump liquid around, which is shown in our paper for the first time.

Here, we report on spherical polyelectrolyte brushes attached to silica micro-sized particles loaded with photosensitive surfactant. We demonstrate that such functionalized brushes can be made to be active in response to an interaction potential when exposed to irradiation with light of an appropriate wavelength. This takes place owing to the generation of local-light-driven diffusioosmotic (*l*-LDDO) flow by the particle itself, so that

the radially directed flow results in long-range diffusioosmotic (DO) repulsion between the particles, the strength and duration of which can be easily controlled by the intensity of the applied light [40]. The photosensitive surfactant consists of cationic head connected through a spacer of six CH₂ groups to an azobenzene molecule having a butyl tail [41]. Owing to the presence of azobenzene in the hydrophobic tail, depending on the wavelength of the applied irradiation, the surfactant can be brought reversibly into two distinct states: a more hydrophobic *trans* one and a more hydrophilic *cis* one [42]. We have demonstrated that, depending on the isomer state, the surfactant molecules prefer to be either within charged confined geometry (*trans* isomers) such as pores in colloidal particles [43], the charged interior of microgel [44,45], planar polyelectrolyte brushes [46,47], linear polyelectrolyte chains [48,49], and other types of surfaces (plain glass and Teflon, hair, nails, sand, and so on) [50,51], while *cis* isomers readily leave and prefer to state in the bulk. The reversible uptake and release of the surfactant molecules builds up the concentration gradient of surrounding isomers, and in the case of objects sedimented at the solid/liquid interface, the corresponding gradient in osmotic pressure establishes fluid motion [52]. An ensemble of such particles function via diffusioosmotic flows establishing the range, the strength, and even the sign of interaction potential and may form either a sparse or a densely packed 2D crystalline-like pattern [53].

Using the example of a poly(methacrylic acid) (PMAA) spherical brush, we have found that the dynamic exchange of the isomers within the brush depends strongly on the light intensity having its critical value at 4 mW/cm², where it is defined by three major points: limited diffusivity of the isomers in the PE layer during light illumination, reduced *trans*–*cis* isomerization kinetics inside the PE layer, and *trans* isomer adsorption reduction towards the PE layer. All these factors result in a reduction in the effective strength of DO flow although the SPBs have a high absorbance tendency in comparison to plain colloids.

The paper is structure as follows: (1) we describe the triggering of the synthesized spherical brushes' photo-responsiveness by loading them with azobenzene containing a surfactant; (2) we study the generation of the local-light-driven diffusioosmotic flow by the brushes and how the strength of the flow depends on irradiation parameters; (3) we compare the behavior of the spherical brushes with porous and plain colloids.

2. Experimental Part

Acetic acid, 3-aminopropyltriethoxysilane (APTS), 2-bromo-2-methylpropionyl bromide (BIBB), ethyl acetate, copper(I)bromide (99.99%), dichloromethane (DCM), hydrochloric acid, N,N,N',N'',N'''-pentamethyl diethylenetriamine (PMDETA), tert-butyl methacrylate (tBuMA), toluene, trifluoroacetic acid (TFA), and sodium hydroxide are purchased from Sigma-Aldrich and used without further purification.

Non-porous silica particles (4.00 ± 0.14 μm) and porous particles (4.9 ± 0.5 μm) are purchased from microParticles GmbH (Germany) and dialyzed five times against 5 L Millipore water.

Poly(methacrylic acid)-coated particles SiO₂@PMAA (Figure 1f) are synthesized as described elsewhere (for more details, see Supporting Information, Section S1) [54]. In short, the surface initiator is first grafted onto the particle surface to allow for a subsequent "grafting from" polymerization. The amino functionalization is performed with 3-aminopropyltriethoxysilane (APTS) in acidic water and then reacted in toluene with 2-bromo-2-methylpropionyl bromide (BIBB) to attach the initiator group on the surface. For polymerization, we utilize surface-initiated ATRP with Cu(I)Br as the catalyst and PMDETA as the ligand in a methanol–water mixture ($V_{\text{MeOH}}/V_{\text{H}_2\text{O}} = 4:1$), keeping the particle concentration low to avoid the fusion of polymer chains from different particles. Polymerization is performed with a high monomer and Cu to initiator molar ratio, and the monomer concentration is set to 122 mM of tert-butyl methacrylate (tBuMA) per reaction batch. Anionic polyelectrolyte brushes are obtained by the polymerization of tBuMA and subsequent hydrolysis in DCM/TFA (trifluoroacetic acid) to obtain poly(methacrylic acid) brushes (SiO₂@PMAA). After the reaction, polymer-coated SiO₂ particles are transferred

into water by dialysis, and charged by adjusting the solution pH to 9. A schematic representation of the synthesis is depicted in Figure S1, Supporting Information. The molecular parameters of the spherical polymer brushes are grafting density of ca. 0.5 nm^{-2} and molecular weight of $7 \cdot 10^4 \text{ g/mol}$ (details of the calculation are presented in Section 1, Supporting Information). The measurements are performed at $\text{pH} = 6$.

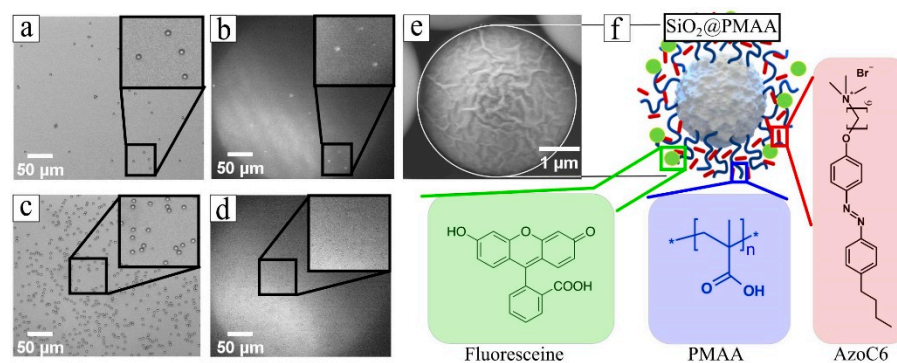


Figure 1. (a–d) Optical micrographs in transmission (a,c) and emission mode for silica colloids loaded with fluorescein and photosensitive surfactant: (a,b) SiO₂@PMAA and (c,d) SiO₂. (e) SEM micrographs of SiO₂@PMAA coated with polymer layer. (f) Scheme of the PMAA (blue lines) spherical brush loaded with surfactant (red rods) and fluorescein (green spheres) and corresponding chemical structures of cationic azobenzene containing surfactant (C₄-azo-OC₆-TMAB, red), poly(methacrylic acid) chain (blue), and fluorescein (green).

Light responsive surfactant. The azobenzene containing trimethyl-ammonium bromide surfactant (C₄-Azo-OC₆-TMAB) is synthesized as described elsewhere [48]. The surfactant (Figure 1f) consists of a spacer of 6 methylene groups between the positively charged trimethylammonium bromide head group and the azobenzene unit with butyl tail attached. A stock solution of surfactant is adjusted to the concentration of 10 mM and diluted to the required sample concentrations ranging from 0.1 to 2 mM. The aqueous dispersion of all particles is mixed with surfactant stock solution and Millipore water at different concentrations and kept at least 1 day for equilibration. A flow chamber with a volume of 40 μL is used in order to provide a closed environment. All samples are kept in the dark or in red light to prevent unwanted photo-isomerization.

Sample preparation for AFM height investigation to estimate brush height. The polydimethylsiloxan (PDMS) film with embedded colloidal SiO₂@PMAA is prepared by cast molding using commercial Sylgard 184 (Dow Corning). This is performed by mixing elastomer and curing agent in a ratio of 10:1, pouring the mixture onto the polymer colloidal spheres, and curing it for 24 h at RT. The films are then detached from the substrate and deposited backwards on the glass slide.

Atomic force microscopy measurements. The AFM measurements are carried out using an NTEGRA AFM (NT-MDT) operating in intermittent contact mode. Commercial tips (Nanoworld-Point probe) with a resonance frequency of 320 kHz and a spring constant of 42 N/m are used.

Optical imaging. Image acquisition is performed in video-recording mode at a monitoring speed of 1 frame per second with an Olympus IX73 equipped with a commercial double monochromatic LED light source (Thorlabs; for blue, $\lambda = 455 \text{ nm}$, M455 L2-C1; for red, $\lambda = 625 \text{ nm}$, M625 L2-C), where images are monitored with a Hamamatsu Camera ORCA-Flash 4.0 LT. The samples are kept in the dark to prevent uncontrolled isomerization. The motion of silica particles on a glass substrate is studied under illumination from above with monochromatic light of $\lambda = 455 \text{ nm}$ (blue) and $\lambda = 625 \text{ nm}$ (red) wavelength. The intensity of irradiation is measured at the sample position ranging from 0.1–50 mW/cm^2 .

Particle motion is tracked using the Mosaic Single Particle Tracking plugin for ImageJ (Rasband, W.S., ImageJ, U. S. National Institutes of Health, Bethesda, MD, USA) [55]. Motion analysis and calculation has been implemented in Matlab.

Thermogravimetric analysis (TGA) is performed using thermal analysis TGA/DTA L81 to 1500 °C (Linseis). In a typical measurement, previously dried samples of SiO₂ and SiO₂@PMAA are heated in a synthetic air environment over a temperature range of 20–800 °C and a heating rate of 10 °C/min.

Zeta potential is calculated from the electrophoretic mobility measured using commercial zetasizer (Nano-ZS, Malvern Instruments, Ltd., Malvern, UK). Prior samples are exposed for 12 min under irradiation with light of the desired wavelength ($I = 10 \text{ mW/cm}^2$), followed by sonication for 10 s.

UV-Vis spectroscopy (Cary 5000 UV-Vis-NIR spectrophotometer, Agilent Technologies, USA) is used to measure the amount of surfactant absorbed by the particles.

Calculation of the amount of adsorbed surfactant: samples are prepared in a manner similar to that previously described, where the surfactant and particle concentration is adjusted to 2 mM and 0.01 mg/mL, respectively. The sample is illuminated by light ($\lambda = 455 \text{ nm}$) with an intensity of 10 mW/cm^2 for 15 min, followed by centrifugation for 1 min. The collected supernatant is diluted 100 times and measured using a UV-Vis spectrometer. The concentration of adsorbed surfactant is calculated via:

$$c_{\text{ads}} = c_{\text{surf}} - c_{\text{UV-Vis}} \cdot 100 \quad (1)$$

with c_{ads} , c_{surf} , and $c_{\text{UV-Vis}}$ as the adsorbed, adjusted, and measured surfactant concentration. $c_{\text{UV-Vis}}$ is calculated using the Beer–Lambert law. Details for the calculation are presented in the Supporting Information, Section S4.

SEM micrographs are recorded with a commercial ZEIS ULTRA PLUS-40-61 microscope.

3. Results and Discussion

Spherical brushes consisting of silica core and poly(methacrylic acid) (PMAA) tethered chains (Figure 1f) are synthesized using an ATRP reaction as described elsewhere (Figure S1, Supporting Information) [54]. The molecular weight of the PMAA chains is fixed to $70 \cdot 10^3 \text{ g/mol}$ according to the synthesis parameters as reported for similar brushes (PMMA) on planar interfaces [56]. To calculate the grafting density we utilize two approaches. By measuring the dry thickness of the scratched brush ($\sim 36 \text{ nm}$) on the colloid (see Section S2, Supporting Information) utilizing AFM for both scratching and cross-section analysis, we estimate the grafting density of the brush to be $(0.39 + 0.01) \text{ nm}^{-2}$. The estimation of the grafting density using gravimetric analysis yields the value $(0.58 + 0.20) \text{ nm}^{-2}$ (Section S2, Supporting Information). Both methods used in our study have several internal error sources, and can be used only to produce an estimate of the grafting density. In the case of the AFM method, the thickness measurements are atomically precise, but the measurements are conducted only on a small number of particles and are thus lacking in the statistics of the system. In the case of gravimetric analysis, a significant contribution to the measurement error is made by the unknown amount of water stored at the oxide surface of the plain particles and within the polyelectrolyte layer of the spherical brushes. However, both methods provide grafting density values that are reasonable for the ATRP process [56].

The supramolecular complex between the spherical brush and the oppositely charged cationic surfactant is formed when the particles are exposed to a surfactant solution for a certain loading time, similar to the situation with a planar poly(methacrylic acid) (PMAA) brush [46,47]. The surfactant molecules penetrate the spherical PMAA brush and form the complex by electrostatic and hydrophobic interactions, replacing the native counterions within the brush interior [57]. This can be observed using the fluorescent signal emitted from the spherical brush and not visible at the plain colloids (compare Figure 1b,d). Here, we make use of the complex formation between a negative charge of fluorescein dye and a cationic surfactant. This complex effectively penetrates into the PE layer, resulting in enhanced emission. Depending on the amount of the adsorbed surfactant, one can also achieve an overcharging of the spherical brush from negatively to positively charged at concentrations of ca. 0.3 mM ($\text{CMC}_{\text{trans}} = 0.5 \text{ mM}$) as measured from the Z-potential (Figure S4, Supporting Information). These results are in good agreement with the previous

study, where it is shown that the complexation of the CTAB surfactant with a poly(styrene sulfonate) spherical brush takes place much below CMC [20].

Since the surfactant is photo-responsive, one can trigger its desorption out of the brush using light. Indeed, when the spherical brushes are irradiated with blue ($\lambda = 455$ nm) or UV ($\lambda = 365$ nm) light ($\tau_{\text{irr}} = 10$ min, $I = 10$ mW/cm²), the surface potential consecutively decreases for all surfactant concentrations, being more pronounced for UV light (Figure S4, Supporting Information). Similar behavior is also observed for charged microgels containing PAA chains and loaded with the azobenzene containing surfactant [58].

The light-triggered reversible adsorption/desorption of the surfactant results in the generation of the concentration gradient around the particles, which leads to a diffusioosmotic flow similar to the microgels (Figure 2) [44]. Here, SiO₂@PMAA are exposed to an aqueous solution of azobenzene containing surfactant ($c_{\text{azo}} = 2$ mM) and placed in a closed chamber in the optical microscope. Without irradiation (imaging proceeds under red light ($\lambda = 625$ nm), with no surfactant photo-isomerization), the sedimented particles move randomly near a surface. Depending on the surfactant concentration one can find the particles in different states: forming aggregates in case of charge compensation and as a single specimen at low and large amounts of surfactant in solution. The number of aggregates decreases with increasing surfactant concentration owing to the overcharging of the brush and electrostatic repulsion. When the irradiation with blue light ($\lambda = 455$ nm) is switched on, the particles start to repel each other until they reach an equilibrium position (Figure 3c,e), as in the case of porous particles [51]. During the whole irradiation time, the particles are essentially trapped at their position, with residual fluctuations due to Brownian motion. The separation distance can be as high as several diameters of the colloid.

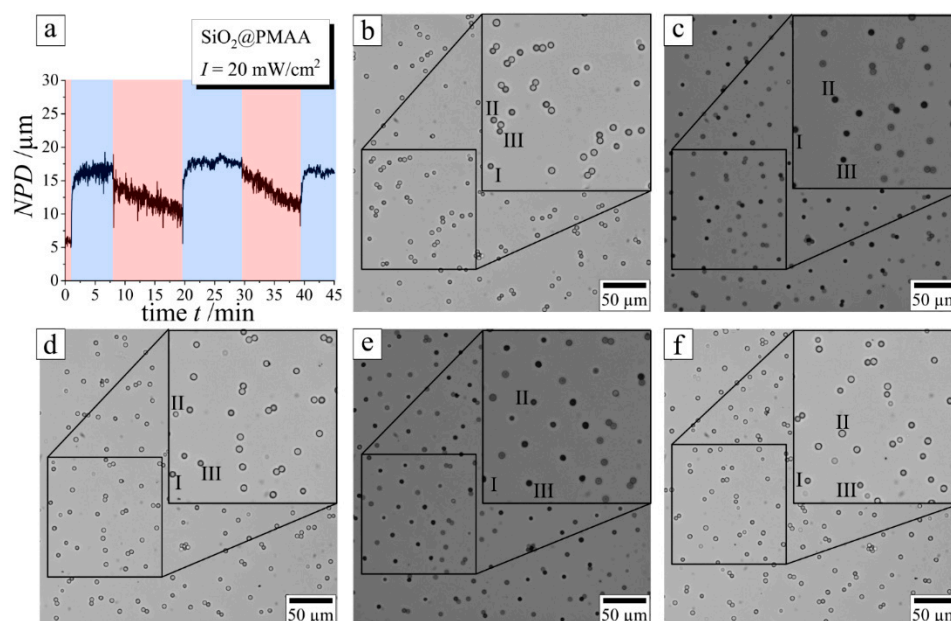


Figure 2. (a) Nearest particle distance (NPD) as a function of the irradiation wavelength and time. Red (625 nm) and blue (455 nm, $I = 20$ mW/cm²) color illustrates the illumination wavelength; (b–f) snapshots of optical micrographs taken at different irradiation steps: (b) at the end of particle aggregation under red illumination (1 min), (c) end of particle separation under blue illumination (5 min), (d) slow particle aggregation at 15 min, (e) fully separated state under blue illumination (25 min), (f) slow particle aggregation during the second cycle (39 min). The corresponding video is provided in Video S1, Supporting Information. Roman numbers I–III illustrate particle position at different recorded optical micrograph snapshots.

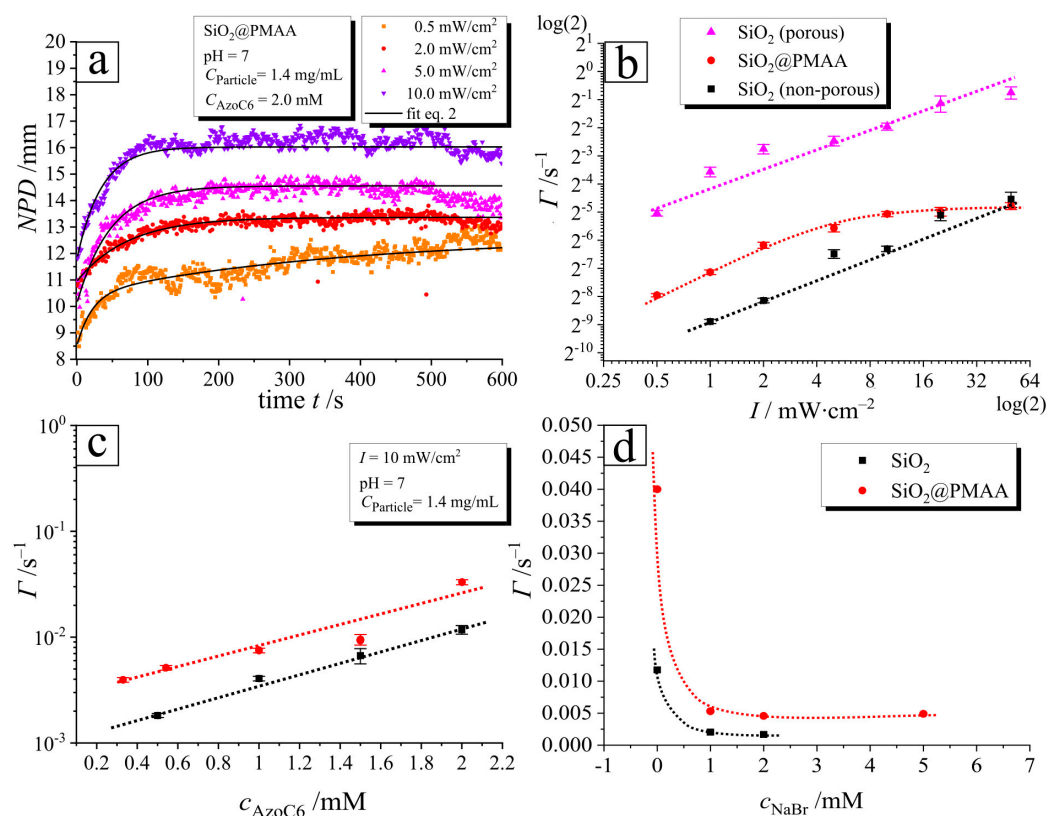


Figure 3. (a) Dependence of NPD on irradiation time ($\lambda = 455$ nm, $I = 10$ mW/cm², $c_{azo} = 2$ mM) for different intensities as indicated in the legend. Black curve depicts exponential fit of the data. The corresponding videos are provided in Videos S2–S6, Supporting Information. (b) Separation rate as a function of intensity for three different particles: porous silica (magenta line), spherical brushes (SiO₂@PMAA, red line), and plain silica colloids (black line). (c,d) Separation rate of SiO₂@PMAA and SiO₂ particles as a function of (c) surfactant concentration and (d) salt concentration (fixed parameters: $I = 10$ mW/cm², $\lambda = 455$ nm, $c_{azo} = 1$ mM, $c_{particle} = 1.4$ mg/mL).

After switching off the light, the long-range diffusioosmotic repulsion basically vanishes, and the particles move freely, undergoing thermal motion (Figure 2a,d,f). To quantify the extend of lateral repulsion, we calculate the nearest particle distance (NPD) as a function of the irradiation time, where NPD is defined as the smallest average distance to a neighboring particle (Figure 2a).

To investigate the flow strength as a function of applied intensity at a fixed wavelength (455 nm), we fit example data displayed in Figure 3a directly after switching the blue light with a single exponential decay function:

$$NPD = NPD_0 + (NPD_e - NPD_0) \cdot \exp(-\Gamma \cdot t) \quad (2)$$

where NPD_e and NPD_0 are the nearest particle distance at the equilibrated and initial state, respectively, t the time, and Γ the characteristic separation rate. Doubling the intensity leads to an almost doubled separation rate, indicating that the DO is linearly proportional to the light intensity up to a critical intensity of 4 mW/cm² (Figure 3b). Beyond this intensity, the separation rate is effectively constant. Data measured for SiO₂@PMAA are compared with data for porous (P -SiO₂) and non-porous (SiO₂) silica colloids of similar size but otherwise unmodified. The porous particles have a pore size of 6 nm and thus a much larger surface area compared to plain colloids. This results in a large amount of surfactant being absorbed by porous particles compared to plain SiO₂ and spherical brushes (SiO₂@PMAA). The separation takes place within seconds or minutes, depending on the light intensity or the particle type (Figure 3b). All particles show the same trend;

with increasing intensity, an increase in the separation can be observed in the following order: $P\text{-SiO}_2 > \text{SiO}_2\text{@PMAA} > \text{SiO}_2$, but without any pronounced velocity limitation at high intensities for SiO_2 and $P\text{-SiO}_2$ (Figure 3b).

We explain the formation of the local diffusioosmotic flow ($I\text{-LDDO}$) for PE-coated particles by the dissimilar photoisomerization rate of the surfactant inside the PE brush and in the bulk, which creates an excess of *cis* isomer concentration Δc_C near the colloids in comparison to the bulk solution. We have demonstrated that the DO flow velocity scales linearly with $\Delta c_C(t)$, where the dependence of Δc_C on time can be estimated by solving the equation [51]:

$$\frac{d\Delta c_C}{dt} \sim I \cdot [k_{\text{TC},I} \cdot c_{\text{T},I} - (k_{\text{TC}} \cdot c_{\text{T},B} - k_{\text{CT}} \cdot c_{\text{C},B})] \quad (3)$$

where $k_{\text{TC},I}$ and k_{TC} are the rate constants of *trans*–*cis* isomerization inside the microgel and bulk solution, respectively, k_{CT} the rate constant of *cis*–*trans* isomerization in the bulk, $c_{\text{T},I}$ the *trans* isomer concentration at the interface, $c_{\text{T},B}$ and $c_{\text{C},B}$ the concentrations of *trans* and *cis* isomers in the bulk, and I the intensity of the light. Here, we interpret the PE brush layer as a diffusive interface capable of absorbing a certain amount of *trans* isomers, larger than in the case of the plain particles (SiO_2), but less than in the case of the porous colloids ($P\text{-SiO}_2$) (see Figure 4a, where the adsorbed amount of the surfactant is shown for three different particles) (for calculations, see Section 4, Supporting Information). When exposed to blue light, more surfactants are released ($c_{\text{released}} \sim c_{\text{dark}} - c_{\text{blue}}$) from the $P\text{-SiO}_2$ ($c_{\text{released}} = 0.03$ mM) than from the $\text{SiO}_2\text{@PMAA}$ ($c_{\text{released}} = 0.02$ mM) and fewer from the plain particles ($c_{\text{released}} = 2 \cdot 10^{-4}$ mM). Furthermore, normalizing the adsorbed surfactant for the $P\text{-SiO}_2$ and the $\text{SiO}_2\text{@PMAA}$ against the SiO_2 shows that the $P\text{-SiO}_2$ absorbs ~ 33 and the $\text{SiO}_2\text{@PMAA}$ ~ 12.5 times more surfactant in comparison to the SiO_2 (dark state, Figure 4b), but under blue illumination (455 nm) the ratio is reduced for the $P\text{-SiO}_2$ to ~ 29 and for the $\text{SiO}_2\text{@PMAA}$ to ~ 9 , where the normalized separation $\Gamma/\Gamma_{\text{SiO}_2}$ (red data, Figure 4b) is congruent for the $P\text{-SiO}_2$ ~ 28.6 but not for the $\text{SiO}_2\text{@PMAA}$ to be ~ 3 and therefore a factor 3 smaller than the value for adsorbed $c_{\text{ads}}/c_{\text{ads,SiO}_2}$. Additionally, data in Figure 3b indicate a linear dependence between the DO flow strength and the surfactant storage capacity for porous silica particles (Equation (3)). For the $\text{SiO}_2\text{@PMAA}$, in principle, all counterions can be replaced by the surfactant molecules, which leads to a strong collapse of the polyelectrolyte brush [46,47]. Thus, technically, a high amount of surfactant molecules can be stored within the PE, and much faster separation compared to plain silica particles should be expected. However, the data yield only three times faster separation (relative particle separation in Figure 4b). Thus, what is causing the pronounced exchange limitation of the isomers even at a high surfactant storage capability?

This can be visualized by considering the exchange and isomerization kinetics of the isomers, which are in cross-correlation from three possible major interactions of the isomers with the PE brush. Indeed, first, the adsorption rate of the *trans* isomer to the polymer (shown on an example of p(NIPAM-MAA) microgels) is 22% slower than to plain silica interfaces ($k_{\text{a,MG}} \sim 7 \text{ L} \cdot (\text{mol} \cdot \text{s})^{-1}$ vs. $k_{\text{a,glass}} = 9 \text{ L} \cdot (\text{mol} \cdot \text{s})^{-1}$ [49,58]. Additionally, the photo-isomerization rate of the surfactant in the aggregate (micelle, restricted geometry) is lower in comparison to non-aggregated molecules owing to steric hindrance [59]. The isomerization rate reduction for blue light (455 nm) is reported for PE-surfactant complexes for single chains [49] ($k_{\text{TC,PE}} = 3 \cdot 10^{-3} \text{ cm}^2 \cdot (\text{mW} \cdot \text{s})^{-1}$) or charged microgels [58] ($k_{\text{TC,MG}} = 2 \cdot 10^{-3} \text{ cm}^2 \cdot (\text{mW} \cdot \text{s})^{-1}$) in comparison to the bulk solution value ($k_{\text{TC,B}} = 8 \cdot 10^{-3} \text{ cm}^2 \cdot (\text{mW} \cdot \text{s})^{-1}$), showing a reduction of $[1 - (k_{\text{TC,PE}}/k_{\text{TC,B}})] = 0.62$. Note that the surfactant molecules in PE layer are in the aggregated state. Finally, a slower diffusivity of the isomers within the PE layer may contribute to the limitation of the isomer exchange. For instance, the generated *cis* isomers localized near the core (see Figure 4c) (1) have a longer diffusion distance across the PE layer than those located at the PE/solution interface (2). For the isomers at location (1), the diffusion time may be equal or larger compared to the rate of *cis*-to-*trans* isomerization thus hindering the *cis* isomer release out of the polymer interior. In comparison, at the position (2), the diffusion time is smaller

and *cis* isomers have enough time to be released into the bulk solution to contribute to the *local*-LDDO flow. Note that the release of surfactant molecules will be compensated by adsorbing counterions, and a swelling of the brush may extend the length of the brush layer, thereby also increasing the diffusion time. These processes become more pronounced with increasing intensity and may explain the marked separation limitation beyond a critical intensity of $4 \text{ mW}/\text{cm}^2$, which is similar to the recently reported value of $3 \text{ mW}/\text{cm}^2$ for microgels, versus no separation limitation of plain and porous silica particles [51].

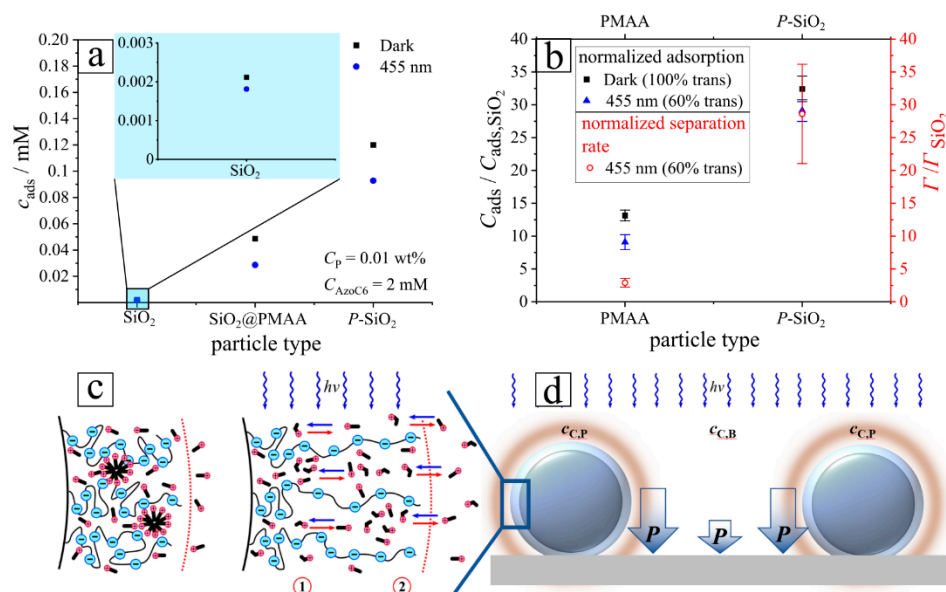


Figure 4. (a) Amount of adsorbed surfactant by three different particle types in dark (black points) and under illumination with blue light ($I = 10 \text{ mW}/\text{cm}^2$, blue points). Surfactant concentration is fixed to 2 mM and particle concentration at $0.14 \text{ mg}/\text{mL}$. (b) Relative adsorption normalized to plain particles (SiO_2) (■ no illumination, ▲ blue light); red dots: average relative particle separation. (c) Cartoon of possible interaction mechanism: left, no illumination; right, under blue light. (d) Cartoon of *l*-LDDO flow generation. “P” indicates osmotic pressure distribution.

The above discussed points effectively reduce the dynamic exchange of isomers between the PE layer and the bulk; therefore, the DO flow $\sim \Delta c_C$ does not scale linearly with surfactant storage capacity for the $\text{SiO}_2@PMAA$, while for the SiO_2 interfaces, one observes a linear relation, $\frac{d\Delta c_C}{dt} \sim c_{T,I}$.

The extent of the DO flow also depends on the surfactant concentration (Figure 3c) and ionic strength (Figure 3d). The dependence of the DO flow on salt concentration is explained by the scaling of the DO velocity with the squared value of the Debye length: as the ionic strength is increased, the EDL thickness decreases and the DO flow vanishes [52,60]. The surfactant concentration dependence can be understood from cross-correlating the dynamic exchange ability of *trans* and *cis* isomers. Assuming the simplest form of adsorption isotherm, the Langmuir relation [50], the rate of *trans* adsorption increases with increasing *trans* isomer concentration in bulk solution, while the rate of *cis* desorption is proportional to the amount of adsorbed *cis* isomers. Since a higher *trans* isomer adsorption rate yields a higher amount of adsorbed *trans* isomers at the interface, more surfactant molecules can be isomerized per time, and therefore more *cis* isomers are temporarily located at the interface and are quickly desorbed into the bulk solution. Thus, the dynamic exchange between *trans* and *cis* isomers is a function of the total surfactant concentration, where an increase in surfactant concentration yields an increase in the amount of exchanged isomers and ultimately a higher induced *cis* isomer gradient during light illumination. However, for the $\text{SiO}_2@PMAA$ particles, the dynamic exchange ability is more complex than at the

plain interface; as described above, a similar trend of flow-strength increase with surfactant concentration is observed (Figure 3c).

4. Conclusions

We report on remotely controlled long-range repulsive interactions between microparticles with a polyelectrolyte (PE) brush coating. The mechanism of DO repulsion is based on the generation of a local-light-driven diffusioosmotic flow, when spherical brushes are exposed to light of an appropriate wavelength. To trigger photoactivity in the spherical polyelectrolyte brushes, azobenzene containing surfactant is loaded within the PE layer. The PMAA brush readily absorbs cationic photo-sensitive surfactant in its more hydrophobic *trans* state and effectively releases more hydrophilic *cis* isomers, resulting in the permanent exchange of the isomers during illumination. The excess of the *cis* isomers near the SPB results in an osmotic pressure gradient and the subsequent formation of the diffusioosmotic flow pointing radially out of the particles. Thus, each spherical brush produces its local lateral diffusioosmotic flow, resulting in hydrodynamic interactions and mutual long-range repulsion. We have also thoroughly analyzed the behavior of the porous particles and spherical brushes in comparison to the plain silica particles exposed to the same irradiation and solution conditions. We have found that the amount of the adsorbed surfactant for porous particles and spherical brushes is ~ 33 and ~ 12.5 times larger than for the plain colloids, respectively. This is reflected also in a more effective generation of the local DO flow. Indeed, for the porous particles we measured a ca. 29 times larger normalized separation $\Gamma/\Gamma_{\text{SiO}_2}$ under irradiation with blue light. However, in the case of the spherical brushes, the DO flow extent increases only by three times (in comparison to the plain particles). We explained this by the fact that the dynamic exchange of the isomers under irradiation with blue light is limited by a reduced *trans* isomer adsorption tendency together with a reduced *trans*–*cis* isomerization rate inside the brush; both processes are weaker in comparison to pure porous silica interfaces. This indicates that the DO flow is limited at a critical light intensity of 4 mW/cm^2 . In summary, photosensitive surfactant is a simple and powerful tool to effectively separate polymer particles without applying any mechanical stresses. This might be an effective application for the separation of unwanted aggregation, which is an often-faced critical phenomenon in colloid and surface science.

Supplementary Materials: The following supporting information can be downloaded at: <https://www.mdpi.com/article/10.3390/pr11030773/s1>. Video S1 represents data to corresponding Figure 2a. Figure S1: Scheme of the poly(methacrylic acid) brush (SiO_2 @PMAA) synthesis on silica colloid. Figure S2: Thermo gravimetric analysis data of bare silica particles (SiO_2) and poly(methacrylic acid)-coated silica particles (SiO_2 @PMAA). Figure S3: Details about polymer height measurements on silica colloids via AFM. Figure S4: Zeta potential of SiO_2 @PMAA for different wavelengths. Figure S5: Adsorption spectra of supernatant surfactant solution: (a) no illumination, (b) blue, (c) UV. Figure S6: Nearest particle distance (NPD) as a function of time: (a) SiO_2 @PMAA and (b) SiO_2 particles immediately after switching on the blue irradiation (455 nm) with an intensity of 10 mW/cm^2 . Figure S7: Nearest particle distance (NPD) as a function of time: (a) SiO_2 and (b) SiO_2 @PMAA particles immediately after switching on the blue irradiation (455 nm) with an intensity of 10 mW/cm^2 . Figure S8: SEM micrographs of PSiO_2 @PMAA microparticles. Reference [61] are cited in the supplementary materials.

Author Contributions: S.S. designed and supervised the project and wrote the manuscript. M.B. synthesized the brushes, performed optical experiments, analyzed the results, and wrote the manuscript. A.K. performed SEM measurements, S.L. performed AFM experiments, and N.L. synthesized the photosensitive surfactant. All the authors were involved in the preparation of the manuscript. All authors have read and agreed to the published version of the manuscript.

Funding: This research was funded by German Research Foundation, DFG grant number SA 1657/19–1.

Data Availability Statement: The data is available in Supplementary Materials.

Conflicts of Interest: The authors declare no competing financial interests.

References

1. Ballauff, M. Spherical polyelectrolyte brushes. *Prog. Polym. Sci.* **2007**, *32*, 1135. [[CrossRef](#)]
2. Ballauff, M.; Borisov, O. Polyelectrolyte brushes. *Curr. Opin. Colloid Interface Sci.* **2006**, *11*, 316–323. [[CrossRef](#)]
3. Guo, X.; Weiss, A.; Ballauff, M. Synthesis of spherical poly-electrolyte brushes by photoemulsion polymerization. *Macromolecules* **1999**, *32*, 6043–6046. [[CrossRef](#)]
4. Guo, X.; Ballauff, M. Spatial dimensions of colloidal polyelectrolytebrushes as determined by dynamic light scattering. *Langmuir* **2000**, *16*, 8719–8726. [[CrossRef](#)]
5. Schrunner, M.; Haupt, B.; Wittemann, A. A novel photoreactor for theproduction of electrosterically stabilised colloidal particles at largerscales. *Chem. Eng. J.* **2008**, *144*, 138–145. [[CrossRef](#)]
6. Hoffmann, M.; Yan, L.; Schrunner, M.; Ballauff, M.; Harnau, L. Dumbbell-shaped polyelectrolyte brushes studied by depo-larized dynamiclight scattering. *J. Phys. Chem. B* **2008**, *112*, 14843–14850. [[CrossRef](#)]
7. Wang, X.; Xu, J.; Li, L.; Wu, S.; Chen, Q.; Lu, Y.; Ballauff, M.; Guo, X. Synthesis of spherical polyelectrolyte brushes by ther-mo-controlled emulsion polymerization. *Macromol. Rapid Commun.* **2010**, *31*, 1272–1275. [[CrossRef](#)] [[PubMed](#)]
8. Hui, C.M.; Pietrasik, J.; Schmitt, M.; Mahoney, C.; Choi, J.; Bockstaller, M.R.; Matyjaszewski, K. Surface-initiated polymeriza-tion as an enabling tool for multifunctional (nano-)engineered hybrid materials. *Chem. Mater.* **2014**, *26*, 745–762. [[CrossRef](#)]
9. Zhang, M.; Liu, L.; Zhao, H.; Yang, Y.; Fu, G.; He, B. Double-responsive polymer brushes on the surface of colloid particles. *J. Colloid Interface Sci.* **2006**, *301*, 85–91. [[CrossRef](#)]
10. Polzer, F.; Heigl, J.; Schneider, C.; Ballauff, M.; Borisov, O.V. Synthesis and analysis of zwitterionic spherical polyelectrolyte brushes in aqueous solution. *Macromolecules* **2011**, *44*, 1654–1660. [[CrossRef](#)]
11. Pfaff, A.; Shinde, V.S.; Lu, Y.; Wittemann, A.; Ballauff, M.; Müller, A.H.E. Glycopolymer-grafted polystyrene nanospheres. *Macromol. Biosci.* **2011**, *11*, 199–210. [[CrossRef](#)] [[PubMed](#)]
12. Jusufi, A.; Likos, C.N.; Ballauff, M. Counterion distributions and effective interactions of spherical polyelectrolyte brushes. *Colloid Polym. Sci.* **2004**, *282*, 910–917. [[CrossRef](#)]
13. Wittemann, A.; Drechsler, M.; Talmon, Y.; Ballauff, M. High elongation of polyelectrolyte chains in the osmotic limit of spherical poly-electrolyte brushes: A study by cryogenic transmission electron microscopy. *J. Am. Chem. Soc.* **2005**, *127*, 9688–9689. [[CrossRef](#)]
14. Das, B.; Guo, X.; Ballauff, M. The osmotic coefficient of spherical polyelectrolyte brushes in aqueous salt-free solution. *Prog. Colloid Polym. Sci.* **2002**, *121*, 34–38.
15. Christau, S.; Thurandt, S.; Yenice, Z.; von Klitzing, R. Stimuli-responsive polyelectrolyte brushes as a matrix for the attachment of gold nanoparticles: The effect of brush thickness on particle distribution. *Polymers* **2014**, *6*, 1877. [[CrossRef](#)]
16. Kesal, D.; Christau, S.; Krause, P.; Möller, T.; von Klitzing, R. Uptake of pH-sensitive gold nanoparticles in strong polyelec-trolyte brushes. *Polymers* **2016**, *8*, 134. [[CrossRef](#)]
17. Cao, Q.; Zuo, C.; Li, L. Electrostatic binding of oppositely charged surfactants to spherical polyelectrolyte brushes. *Phys. Chem. Chem. Phys.* **2011**, *13*, 9706–9715. [[CrossRef](#)]
18. Riley, J.K.; An, J.; Tilton, R.D. Ionic Surfactant Binding to pH-Responsive Polyelectrolyte Brush-Grafted Nanoparticles in Suspension and on Charged Surfaces. *Langmuir* **2015**, *31*, 13680–13689. [[CrossRef](#)]
19. Lu, Y.; Ballauff, M. Spherical polyelectrolyte brushes as nanoreactors for the generation of metallic and oxidic nanoparticles: Synthesis and application in catalysis. *Prog. Polym. Sci.* **2016**, *59*, 86–104. [[CrossRef](#)]
20. Samokhina, L.; Schrunner, M.; Ballauff, M.; Drechsler, M. Binding of Oppositely Charged Surfactants to Spherical Polyelec-trolyte Brushes: A Study by Cryogenic Transmission Electron Microscopy. *Langmuir* **2007**, *23*, 3615–3619. [[CrossRef](#)]
21. Walkowiak, J.; Lu, Y.; Gradzielski, M.; Zauscher, S.; Ballauff, M. Thermodynamic Analysis of the Uptake of a Protein in a Spherical Polyelectrolyte Brush. *Macromol. Rapid Commun.* **2020**, *41*, 1900421. [[CrossRef](#)] [[PubMed](#)]
22. Gu, S.; Risse, S.; Lu, Y.; Ballauff, M. Mechanism of the Oxidation of 3,3',5,5'-Tetramethylbenzidine Catalyzed by Peroxi-Dase-Like Pt Nanoparticles Immobilized in Spherical Polyelectrolyte Brushes: A Kinetic Study. *ChemPhysChem* **2020**, *21*, 450–458. [[CrossRef](#)] [[PubMed](#)]
23. Li, L.; Li, M.; Qiu, Z.; Chen, K.; Xu, Y.; Guo, X.; Wang, J. Catalytic Activity Comparison of Gold Nanoparticles in Annealed and Quenched Spherical Polyelectrolyte Brushes. *Chem. Lett.* **2022**, *51*, 284–287. [[CrossRef](#)]
24. Sun, L.; Fu, Z.; Ma, E.; Guo, J.; Zhang, Z.; Li, W.; Li, L.; Liu, Z.; Guo, X. Ultra small Pt Nanozymes Immobilized on Spherical Polyelectrolyte Brushes with Robust Peroxidase-like Activity for Highly Sensitive Detection of Cysteine. *Langmuir* **2022**, *38*, 12915–12923. [[CrossRef](#)]
25. Yaroslavov, A.A.; Sybachin, A.V.; Zaborova, O.V.; Migulin, V.A.; Samoshin, V.V.; Ballauff, M.; Kesselman, E.; Schmidt, J.; Talmon, Y.; Menger, F.M. Capacious and programmable multi-liposomal carriers. *Nanoscale* **2015**, *7*, 1635–1641. [[CrossRef](#)] [[PubMed](#)]
26. Wittemann, A.; Haupt, B.; Ballauff, M. Adsorption of proteins on spher-ical polyelectrolyte brushes in aqueous solution. *Phys. Chem. Chem. Phys.* **2003**, *5*, 1671–1677. [[CrossRef](#)]
27. Haupt, B.; Neumann, T.; Wittemann, A.; Ballauff, M. Activity of enzymes immobilized in colloidal spherical polyelectrolyte brushes. *Biomacromolecules* **2005**, *6*, 948–955. [[CrossRef](#)]

28. Henzler, K.; Haupt, B.; Lauterbach, K.; Wittemann, A.; Borisov, O.; Ballauff, M. Adsorption of actoglobulin on spherical polyelectrolyte brushes: Direct proof of counterion release by isothermal titration calorimetry. *J. Am. Chem. Soc.* **2010**, *132*, 3159–3163. [[CrossRef](#)]
29. Rumyantsev, A.M.; Santer, S.; Kramarenko, E.Y. Theory of Collapse and Overcharging of a Polyelectrolyte Microgel Induced by an Oppositely Charged Surfactant. *Macromolecules* **2014**, *47*, 5388–5399. [[CrossRef](#)]
30. Sun, L.; Han, H.; Liu, Z.; Fu, Z.; Hua, C.; Ma, E.; Guo, J.; Liu, J.; Li, L.; Fang, B.; et al. Immobilization of Gold Nanoparticles in Spherical Polymer Brushes Observed by Small-Angle X-ray Scattering. *Langmuir* **2022**, *38*, 1869–1876. [[CrossRef](#)]
31. Mei, Y.; Lauterbach, K.; Hoffmann, M.; Borisov, O.V.; Ballauff, M.; Jusufi, A. Collapse of Spherical Polyelectrolyte Brushes in the Presence of Multivalent Counterions. *Phys. Rev. Lett.* **2006**, *97*, 158301. [[CrossRef](#)]
32. Konradi, R.; Rühle, J. Binding of oppositely charged surfactants to poly (methacrylic acid) brushes. *Macromolecules* **2005**, *38*, 6140. [[CrossRef](#)]
33. Iqbal, D.; Yan, J.; Matyjaszewski, K.; Tilton, R.D. Swelling of multi-responsive spherical polyelectrolyte brushes across a wide range of grafting densities. *Colloid Polym. Sci.* **2020**, *298*, 35–49. [[CrossRef](#)]
34. Sin, J.S.; Choe, I.-C.; Im, C.-S. Electric double layer of spherical pH-responsive polyelectrolyte brushes in an electrolyte solution: A strong stretching theory accounting for excluded volume interaction and mass action law. *Phys. Fluids* **2022**, *34*, 097121. [[CrossRef](#)]
35. Rühle, J.; Ballauff, M.; Biesalski, M.; Dziezok, P.; Gröhn, F.; Johannsmann, D.; Houbenov, N.; Hugenberg, N.; Konradi, R.; Minko, S.; et al. Polyelectrolyte brushes. *Adv. Comput. Simul. Approaches Soft Matter Sci. I* **2004**, *165*, 79–150.
36. Li, M.; Zhuang, B.; Yu, J. Effects of Ion Valency on Polyelectrolyte Brushes: A Unified Theory. *Macromolecules* **2022**, *55*, 10450–10456. [[CrossRef](#)]
37. Guo, X.; Ballauff, M. Spherical polyelectrolyte brushes: Comparison between annealed and quenched brushes. *Phys. Rev. E* **2001**, *64*, 051406. [[CrossRef](#)]
38. Mei, Y.; Ballauff, M. Effect of counterions on the swelling of spherical polyelectrolyte brushes. *Eur. Phys. J. E* **2005**, *16*, 341–349. [[CrossRef](#)] [[PubMed](#)]
39. Quan, G.; Wang, M.; Tong, C. A numerical study of spherical polyelectrolyte brushes by the self-consistent field theory. *Polymer* **2014**, *55*, 6604–6613. [[CrossRef](#)]
40. Feldmann, D.; Arya, P.; Molotilin, T.Y.; Lomadze, N.; Kopyshv, A.; Vinogradova, O.I.; Santer, S. Extremely Long-Range Light-Driven Repulsion of Porous Microparticles. *Langmuir* **2020**, *36*, 6994. [[CrossRef](#)]
41. Arya, P.; Jelken, J.; Lomadze, N.; Santer, S.; Bekir, M. Kinetics of photo-isomerization of azobenzene containing surfactants. *J. Chem. Phys.* **2020**, *152*, 024904. [[CrossRef](#)] [[PubMed](#)]
42. Montagna, M.; Guskova, O. Photosensitive Cationic Azobenzene Surfactants: Thermodynamics of Hydration and the Complex Formation with Poly(methacrylic acid). *Langmuir* **2018**, *34*, 311. [[CrossRef](#)] [[PubMed](#)]
43. Arya, P.; Jelken, J.; Feldmann, D.; Lomadze, N.; Santer, S. Light driven diffusioosmotic repulsion and attraction of colloidal particles. *J. Chem. Phys.* **2020**, *152*, 194703. [[CrossRef](#)]
44. Sharma, A.; Bekir, M.; Lomadze, N.; Jung, S.-H.; Pich, A.; Santer, S. Generation of Local Diffusioosmotic Flow by Light Re-sponsive Microgels. *Langmuir* **2022**, *38*, 6343–6351. [[CrossRef](#)]
45. Jelken, J.; Jung, S.H.; Lomadze, N.; Gordievskaya, Y.D.; Kramarenko, E.Y. Tuning the Volume Phase Transition Temperature of Microgels by Light. *Adv. Funct. Mater.* **2022**, *32*, 2107946. [[CrossRef](#)]
46. Kopyshv, A.; Galvin, C.J.; Patil, R.R.; Genzer, J.; Lomadze, N.; Feldmann, D. Light-induced reversible change of roughness and thickness of photosensitive polymer brushes. *ACS Appl. Mater. Interfaces* **2016**, *8*, 19175–19184. [[CrossRef](#)]
47. Kopyshv, A.; Lomadze, N.; Feldmann, D.; Genzer, J.; Santer, S. Making polymer brush photosensitive with azobenzene containing surfactants. *Polymer* **2015**, *79*, 65–72. [[CrossRef](#)]
48. Zakrevskyy, Y.; Cywinski, P.; Cywinska, M.; Paasche, J.; Lomadze, N.; Reich, O.; Löhmansröben, H.-G.; Santer, S. Interaction of photosensitive surfactant with DNA and poly acrylic acid. *J. Chem. Phys.* **2014**, *140*, 044907. [[CrossRef](#)]
49. Sharma, A.; Bekir, M.; Lomadze, N.; Santer, S. Photo-Isomerization Kinetics of Azobenzene Containing Surfactant Conjugated with Polyelectrolyte. *Molecules* **2021**, *26*, 19. [[CrossRef](#)]
50. Umlandt, M.; Feldmann, D.; Schneck, E.; Santer, S.; Bekir, M. Adsorption of Photoresponsive Surfactants at Solid–Liquid In-terface. *Langmuir* **2020**, *36*, 14009. [[CrossRef](#)]
51. Bekir, M.; Sharma, A.; Umlandt, M.; Lomadze, N.; Santer, S. How to turn any surface to act as a micropump. *Adv. Mater. Interf.* **2022**, *9*, 2102395. [[CrossRef](#)]
52. Feldmann, D.; Maduar, S.R.; Santer, M.; Lomadze, N.; Vinogradova, O.I.; Santer, S. Manipulation of small particles at solid liquid interface: Light driven diffusioosmosis. *Sci. Rep.* **2016**, *6*, 36443. [[CrossRef](#)] [[PubMed](#)]
53. Frenkel, M.; Arya, P.; Bormachenko, E.; Santer, S. Quantification of Ordering in Active Light Driven Colloids. *J. Colloid Interface Sci.* **2021**, *586*, 866–875. [[CrossRef](#)]
54. Sokolowski, M.; Bartsch, C.; Spiering, V.J.; Prévost, S.; Appavou, M.-S.; Schweins, R.; Gradzielski, M. Preparation of Polymer Brush Grafted Anionic or Cationic Silica Nanoparticles: Systematic Variation of the Polymer Shell. *Macromolecules* **2018**, *51*, 6936. [[CrossRef](#)]
55. Sbalzarini, I.F.; Koumoutsakos, P. Feature point tracking and trajectory analysis for video imaging in cell biology. *J. Struc. Biol.* **2005**, *151*, 182–195. [[CrossRef](#)]

56. Patil, R.R.; Turgman-Cohen, S.; Šrogl, J.; Kiserow, D.; Genzer, J. On-demand degrafting and the study of molecular weight and grafting density of poly(methyl methacrylate) brushes on flat silica substrates. *Langmuir* **2015**, *31*, 2372–2381. [[CrossRef](#)] [[PubMed](#)]
57. Schimka, S.; Gordievskaya, Y.D.; Lomadze, N.; Lehmann, M.; Klitzing, R.; Romyantsev, A.M.; Kramarenko, E.; Santer, S. Light driven remote control of microgels' size in the presence of photosensitive surfactant: Complete phase diagram. *J. Chem. Phys.* **2017**, *147*, 031101. [[CrossRef](#)] [[PubMed](#)]
58. Sharma, A.; Jung, S.-H.; Lomadze, N.; Pich, A.; Santer, S.; Bekir, M. Adsorption Kinetics of a Photosensitive Surfactant Inside Microgels. *Macromolecules* **2021**, *54*, 10682–10690. [[CrossRef](#)]
59. Titov, E.; Sharma, A.; Lomadze, N.; Saalfrank, P.; Santer, S.; Bekir, M. Photoisomerization of Azobenzene-Containing Surfactant within a Micelle. *ChemPhotoChem* **2021**, *5*, 926. [[CrossRef](#)]
60. Prieve, D.C.; Anderson, J.L.; Ebel, J.P.; Lowell, M.E. Motion of a particle generated by chemical gradients. Part 2. Electrolytes. *J. Fluid Mech.* **1984**, *148*, 247–269. [[CrossRef](#)]
61. Masalov, V.M.; Sukhinina, N.S.; Kudrenko, E.A.; Emelchenko, G.A. Mechanism of formation and nanostructure of Stöber silica particles. *Nanotechnology* **2011**, *22*, 275718. [[CrossRef](#)] [[PubMed](#)]

Disclaimer/Publisher's Note: The statements, opinions and data contained in all publications are solely those of the individual author(s) and contributor(s) and not of MDPI and/or the editor(s). MDPI and/or the editor(s) disclaim responsibility for any injury to people or property resulting from any ideas, methods, instructions or products referred to in the content.